The variation of the metal/mold heat transfer coefficient along the cross section of cylindrical shaped castings

Eduardo N. Souza, Noé Cheung, Carlos A. Santos & Amauri Garcia

Published online: 22 Aug 2006.

Submit your article to this journal ⬈

View related articles ⬈

Taylor & Francis
Taylor & Francis Group

The variation of the metal/mold heat transfer coefficient along the cross section of cylindrical shaped castings

EDUARDO N. SOUZA, NOÉ CHEUNG, CARLOS A. SANTOS
and AMAURI GARCIA*

Department of Materials Engineering, State University of Campinas,
UNICAMP, Campinas, SP, Brazil

During solidification, the mathematical analysis of heat flow depends on the transient heat transfer coefficient at the metal/mold interface. The analysis of heat transfer behavior along a cylindrical section is necessary for a better control of solidification in conventional foundry and continuous casting processes. For this purpose, a water-cooled experimental apparatus was developed, and experiments were carried out with Sn–Pb alloys with different melt superheats. The heat transfer coefficients were determined by a theoretical–experimental fit of thermal profiles (IHCP). The results have shown a variation in heat flow conditions along the metal/mold interface provoked by the action of solidification thermal contraction connected with the gravitational effect. In macrostructural terms, this effect was evident with an asymmetric structure due to the variation of metal/mold thermal contact along the cylinder cross section. Experimental equations correlating heat transfer coefficients as a power function of time along the cross section of cylindrical horizontal castings of Sn–Pb alloys are proposed.

Keywords: Transient heat transfer; Metal/mold interface; Sn–Pb alloys

1. Introduction

The metal's contraction phenomenon, the physical and chemical characteristics of both metal and mold, and the mold expansion during solidification, are mechanisms which are responsible for the air gap formation in the metal/mold interface. In the beginning of the process, when the metal is completely liquid, the thermal contact is more effective due to the higher fluidity and the metalostatic pressure effects. However, with the evolution of solidification, the thermal contraction generated by the liquid/solid transformation creates a physical space at the interface; in this way, the thermal resistance to the heat flowing into the mold increases. Thus, the thermal behavior of the interface varies with location from the interface and with time as solidification progresses. In addition, the orientation of the casting/mold interface with respect to gravity has a strong

*Corresponding author. Email: amaurig@fem.unicamp.br

influence on the pressure between the casting and the mold surfaces at this interface. For horizontal cylinders, air gap width varies along the cross section during solidification. The weight of the casting results in good thermal contact between the casting and the chill mold at the bottom. The angular contact gradually becomes poorer from the bottom ($\theta = 0°$) to the side ($\theta = 90°$) and top ($\theta = 180°$) along the casting/mold interface.

The importance of determining this interface condition lies in the fact that it decisively influences cooling rate and solidification time in metallic molds. Numerous studies have been devoted to the measurement and determination of this boundary value [1–7]. Some experimental studies [8–10] have determined the transient heat transfer coefficient at the metal/mold interface in cylindrical ingots, but they have not considered the angular variation of the gap along the cross section.

The present work is aimed to implement the approach of the inverse heat transfer calculation, to study the heat transfer during solidification of Sn–Pb alloys in a horizontal cylindrical chilled mold and to determine the time-dependent overall heat transfer coefficient considering the angular variation along the cylinder cross section.

2. Mathematical analysis

The development of the mathematical model is based on the general equation of heat conduction [11] expressed in cylindrical coordinates:

$$\frac{1}{r}\frac{\partial}{\partial r}\left(kr\frac{\partial T}{\partial r}\right) + \frac{1}{r^2}\frac{\partial}{\partial \phi}\left(k\frac{\partial T}{\partial \phi}\right) + \frac{\partial}{\partial z}\left(k\frac{\partial T}{\partial z}\right) + \dot{q} = \rho c \frac{\partial T}{\partial t} \tag{1}$$

where r, z, and ϕ are the cylindrical coordinates represented in figure 1. The term for the heat generation of energy ($\dot{q}$) in the unsteady state condition is:

$$\dot{q} = \rho \mathrm{L} \frac{\partial fs}{\partial t} \tag{2}$$

where fs, is the fraction of solid formed during the phase transformation.

Considering that the flow of heat is mostly radial, equation (1) can be reduced for the one-dimensional form. Thus, the direction z of heat extraction can be neglected,
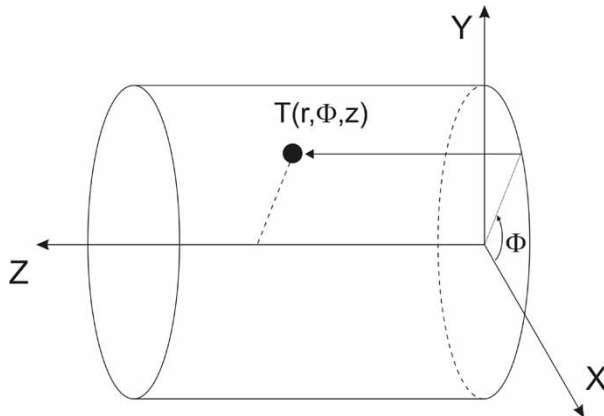

Figure 1.   Cylindrical coordinate system.

once it is not significant regarding the heat flow in the r and ϕ directions. In the case of ingots with a symmetrical section, the heat flow in the ϕ direction can also be neglected, resulting in a simplified equation.

$$\frac{1}{r}\frac{\partial}{\partial r}\left(kr\frac{\partial T}{\partial r}\right) + \dot{q} = \rho c\frac{\partial T}{\partial t} \tag{3}$$

Substituting equation (2) into (3) gives:

$$\frac{1}{r}\frac{\partial}{\partial r}\left(kr\frac{\partial T}{\partial r}\right) = \rho c'\frac{\partial T}{\partial t} \tag{4}$$

where

$$c' = \left(c - L\frac{\partial fs}{\partial T}\right) \tag{5}$$

The term c', known as the pseudo specific heat, accounts for both temperature change as well as the latent heat liberation associated with the phase transformation in the temperature range (T_S, T_L), where T_S is the solidus temperature and T_L is the liquidus temperature.

The terms k, ρ and c' vary with each phase along solidification, i.e. liquid, mush and solid.

Using the finite difference method (FDM) for the development of equation (4), we have:

$$T_i^{n+1} = \frac{\Delta t}{\rho_i c_i' r_i \Delta r^2}\left[k_{i-1}r_i\left(T_{i-1}^n - T_i^n\right) + k_{i+1}r_{i+1}\left(T_{i+}^n - T_i^n\right)\right] + T_i^n \tag{6}$$

for $i \neq 0$.

Where the subscript (i) represents the location of the element in the finite difference mesh and ($n+1$), the instant in that the nodal temperature is being calculated, as represented in the nodal network shown in figure 2.

Considering the metal/mold interface, the following thermal balance can be applied:

$$hA_m(T_a - T_m) + k_{m-1}A_{m-1}\left.\frac{\partial T}{\partial r}\right|_{m-1} = \rho cV\left.\frac{\partial T}{\partial t}\right|_m \tag{7}$$
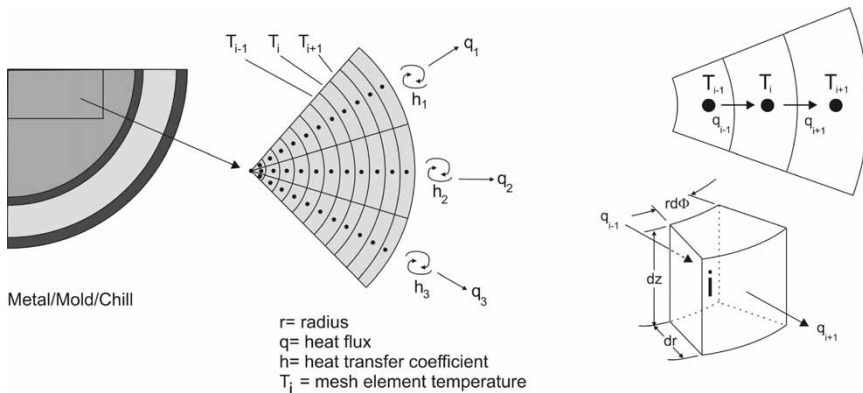

Figure 2.   FDM mesh applied at the cross section of the metal/mold cylindrical system.

where A is the heat transfer area of the finite difference element; V is the volume of the finite difference element;

$$T_{\mathrm{m}}^{n+1} = \frac{\Delta t}{\rho c' r_{\mathrm{m}} \Delta r} \left[h r_{\mathrm{m}} \left(T_{\mathrm{a}}^n - T_{\mathrm{m}}^n \right) + k_{\mathrm{m}} r_{\mathrm{m}-1} \frac{T_{\mathrm{m}-1}^n - T_{\mathrm{m}}^n}{\Delta r} \right] + T_{\mathrm{m}}^n \tag{8}$$

where r_{m} is external radius of the cylindrical ingot; T_{m} is the ingot surface temperature; h is the overall heat transfer coefficient between the casting surface and the coolant fluid [12]:

$$\frac{1}{h} = \frac{1}{h_i} + \frac{e}{k_{\mathrm{m}}} + \frac{1}{h_{\mathrm{W}}} \tag{9}$$

where h_i is the heat transfer coefficient at the metal/mold interface [$\mathrm{W\,m^{-2}\,K^{-1}}$], e is the mold thickness [m], k_{m} is the mold thermal conductivity [$\mathrm{W\,m^{-1}\,K^{-1}}$] and h_{w} is the mold–coolant heat transfer coefficient.

As the solidification proceeds, the contraction of the metal increases forming an air gap at the metal/mold interface, increasing the thermal resistance with the consequent decrease in heat flow. The knowledge of the transient heat transfer coefficient at the metal/mold interface is primordial in the analysis of the solidification process, being necessary its determination. There are several methods to solve this problem. The method based on the theoretical–experimental fit of thermal profiles, used in this work, consists of accomplishing experimental thermal profiles in the mold and/or in the metal along the solidification process and, afterwards, to confront them with those furnished by theoretical solidification heat transfer models [6,7,12,13].

The method used to determine the transient metal/coolant heat transfer coefficient, h, is based on the solution of the inverse heat conduction problem (IHCP) [2,14]. This method makes a complete mathematical description of the physics of the process and is supported by the temperature measurements at known locations inside the heat conducting body. The temperature files containing the experimentally monitored temperatures are used in a finite difference heat flow model to determine h, as described in a previous article [12]. The process at each time step included the following: a suitable initial value of h is assumed and with this value, the temperature of each reference location in casting at the end of each time interval Δt is simulated by using an implicit finite difference technique. The correction in h at each interaction step is made by a value Δh, and new temperatures are estimated $[T_{\mathrm{est}}(h + \Delta h)]$ or $[T_{\mathrm{est}}(h - \Delta h)]$. With these values, sensitivity coefficients (ϕ) are calculated for each interaction, given by:

$$\phi = \frac{T_{\mathrm{est}}(h + \Delta h) - T_{\mathrm{est}}(h)}{\Delta h} \tag{10}$$

The procedure determines the value of h, which minimizes an objective function defined by:

$$F(h) = \sum_{i=1}^{n} (T_{\mathrm{est}} - T_{\mathrm{exp}})^2 \tag{11}$$

where T_{est} and T_{exp} are the estimated and the experimentally measured temperatures at various thermocouples locations and times, and n is the iteration stage.
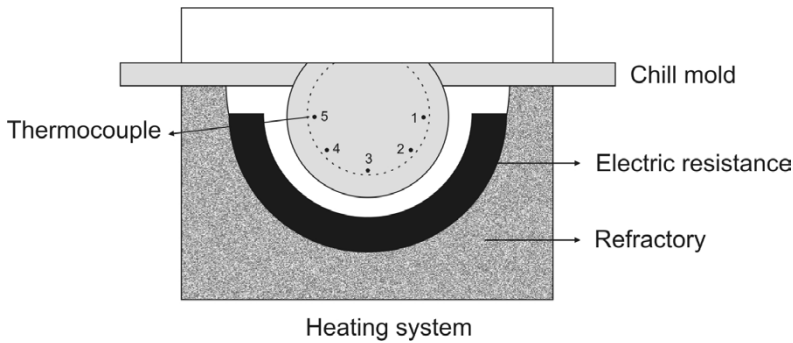
Figure 3. Schematic representation of the experimental setup and thermocouple positions.

3. Experimental procedure

The experimental apparatus consists of a horizontal cylindrical chill made of stainless steel as schematically shown in figure 3. After the metal melts, the mold is taken off of the heating system and is cooled by water.

For monitoring the temperatures, a recording microprocessor system with 16 channels was used and J-type thermocouples (iron–constantan) were placed longitudinally along the section at points located 5 mm from the metal/mold interface and subsequently 45° equidistant of each other, as shown in figure 4. The thermocouples were fixed in a drilled support, with holes of 1.5 mm in diameter. After solidification, the ingot was sectioned and examined to confirm the thermocouple positions. The cooling system was designed in such way that the water flow guarantees an extraction of heat essentially radial during solidification. The water flow was kept constant about $20 \, \text{L} \, \text{min}^{-1}$, controlled by a rotameter. Figure 4 shows a perspective view of the cooled chill mold used in the experiments, while figure 5 shows its cross section with the respective dimensions.

For the experimental analysis, Sn 5wt.% Pb and Sn 15wt.% Pb alloys were used, with melt superheats of 3 and 20% above the liquidus temperature. A solution containing 55 g of $FeCl_3$ and 4 mL HCl for each 150 mL of water was used to reveal the ingot macrostructure. The thermo-physical properties of the alloys used in the simulations performed with the developed solidification model are shown in table 1.

4. Results and discussion

The temperature measurements have shown that the experimental apparatus permitted an essentially constant melt temperature to be attained before the beginning of cooling hence, avoiding different melt superheats inside the casting. As expected, thermocouples 1 and 2 furnished experimental thermal profiles close to those of positions 5 and 4, respectively, due to the ingot symmetry (figure 3). For this reason, only the thermocouples 1 through 3 were considered in the analysis. The columnar structure observed on the longitudinal and radial sections reveals a typical radial heat flow, as shown in figure 6. An asymmetry can be seen in the macrostructure, as well as the end of the solidification that occurs above the geometric center of the casting, indicating
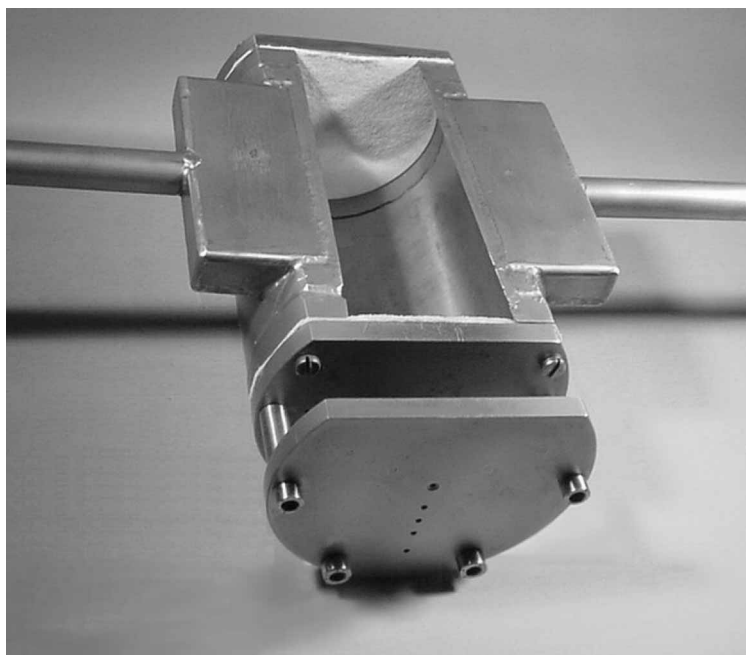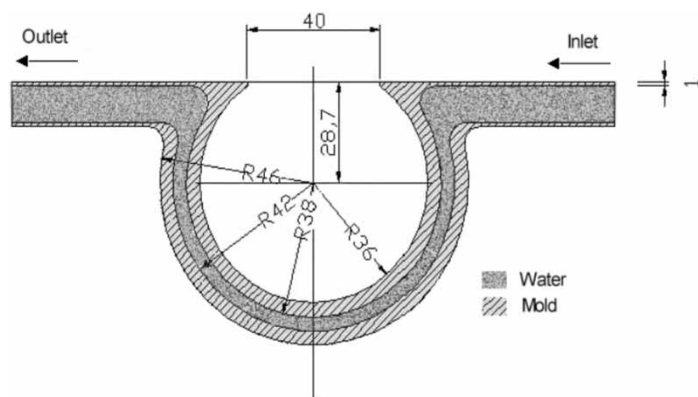
Figure 4.   Stainless steel chill mold.

Figure 5.   Cross section and dimensions of the chill mold [mm].

variation of heat flow at the metal/mold interface along the cylinder cross section. The structure indicates that the heat transfer was more effective at the bottom, decreasing along the cylinder surface toward the top (figure 6).

The effect of metal contraction on air gap formation is better visualized by means of the experimental temperature profiles monitored at different points inside the casting located at 5 mm from the metal/mold interface. The different heat transfer coefficients were determined through an automatic search of the best fit between experimental and numerically predicted thermal profiles, as detailed in a previous article [12].

Table 1. Thermophysical properties [15–18].

	Sn 5wt.%Pb	Sn 15wt.%Pb	Eutetic
k_S	65.4	62.2	54.4
k_L	32.8	32.5	31.7
ρ_S	7184	7906	8875
ρ_L	7184	7551.7	8434
c_S	216.4	207.3	185.4
c_L	253	240.9	211.9
L	58,985	55,534	47,253
T_L	225	210	–
T_E	183	183	183
T_F	232	232	–
K_o	0.0656	0.0656	0.0656
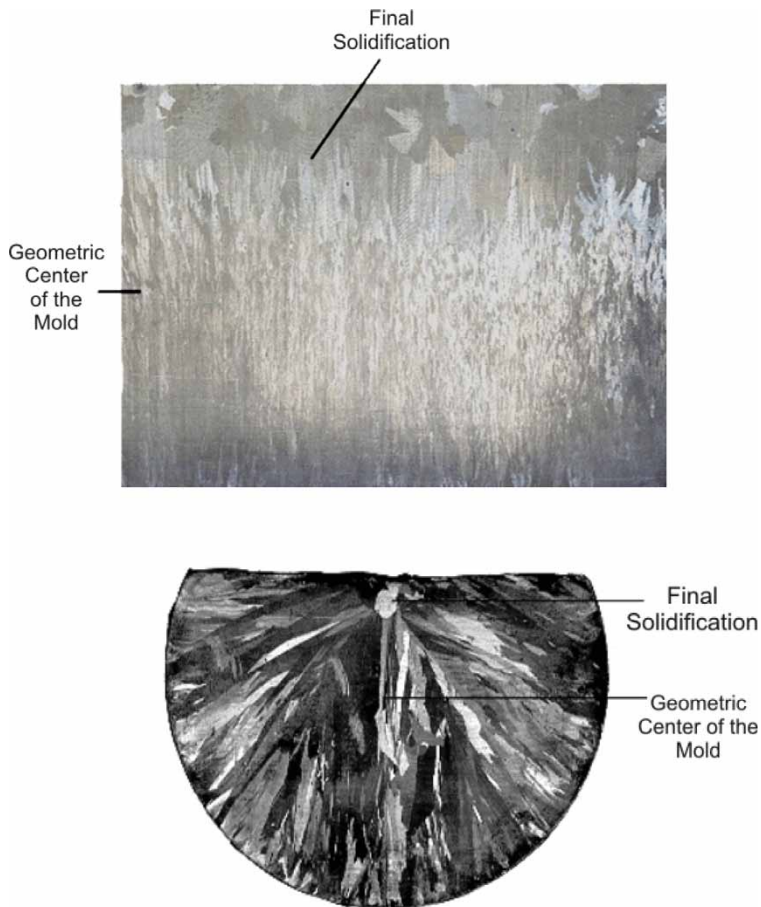
Figure 6. Typical macrostructure (longitudinal and transversal) of the cylindrical casting cross section: Sn 5 wt.% Pb, initial melt temperature $(T_P) = 252°C$. Magnification: $1\times$.
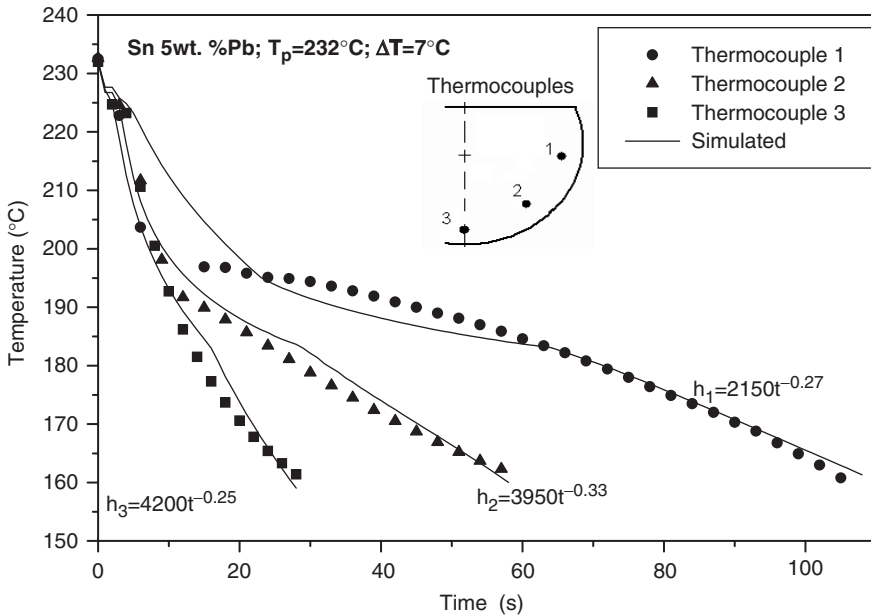
Figure 7. Experimental and simulated temperatures (Sn 5wt.% Pb, $T_P = 232°C$).

Figures 7 through 10 show the comparison between experimental thermal responses and those simulated for the Sn 5wt.% Pb and Sn 15wt.% Pb alloy castings, with 3 and 20% of melt superheat.

The results of thermal analysis show a decrease of the thermal contact between the metal and the mold, with the angular variation toward the casting top. The metal contraction at the ingot bottom is less pronounced than at the other regions due to the the gravitational effect. Tables 2 and 3 show the resulting equations describing the metal/mold transient heat transfer coefficients (h), at characteristic positions along the cylinder cross section. They express h as a power function of time, given by:

$$h = at^{-b}$$

where t is the time; b and a are constants which depend on alloy composition and solidification conditions.

The power regression finds the equation of the form $h = at^{-b}$ that best fits a set of data consisted of values of h *versus* time, determined by the IHCP method. The regression equation is a linearly least-squares fit on the values for $\ln(t)$ and $\ln(h)$ in order to determine the values for constants a and b.

The metal/mold transient heat transfer coefficients expressed as a power function of time can be taken as a general trend, but care should be exercised when applying the expression to the beginning of solidification. A more complex experimental set-up with a higher frequency of temperature acquisition would be necessary for accurate characterization of initial values of heat transfer coefficients (e.g. time < 3 s) for the present experiment.
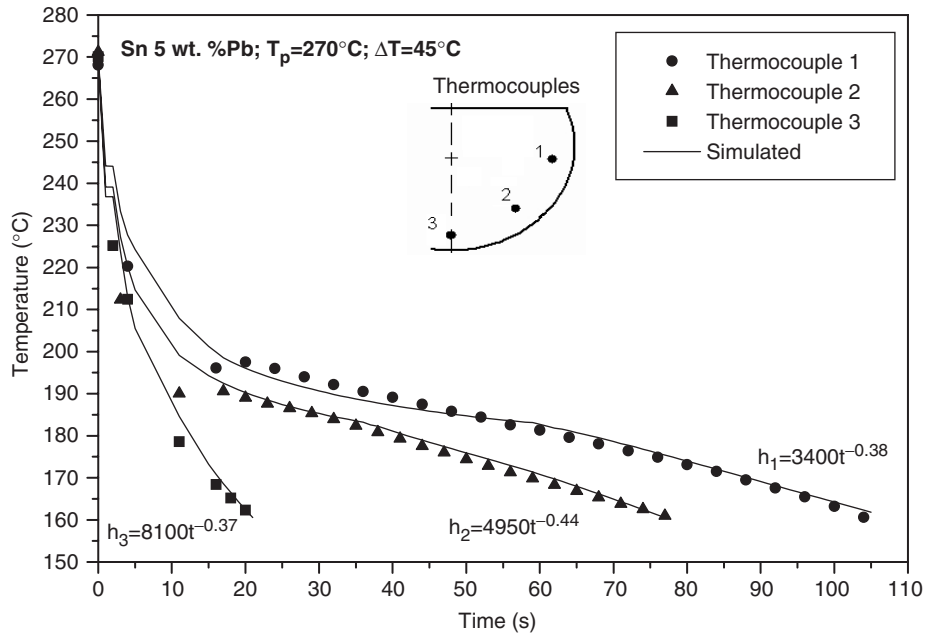
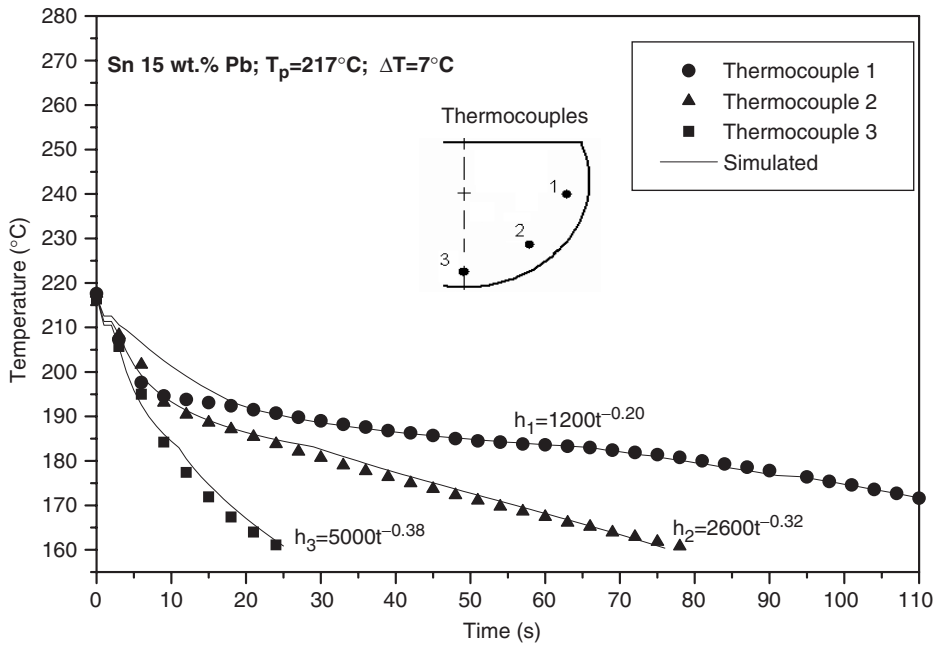Figure 8.   Experimental and simulated temperatures (Sn 5wt.% Pb, $T_P = 270°C$).

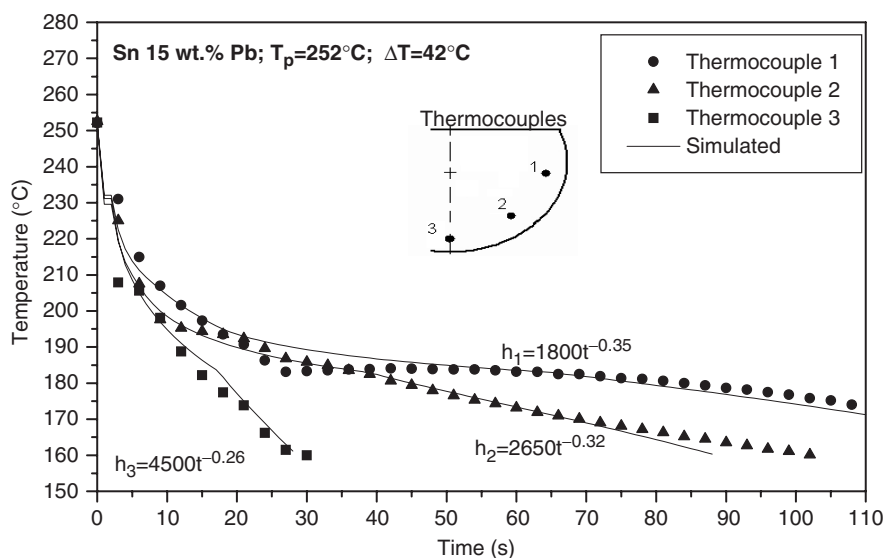Figure 9.   Experimental and simulated temperatures (Sn 15wt.% Pb, $T_P = 217°C$).

Figure 10.   Experimental and simulated temperatures (Sn 15wt.% Pb, $T_P = 252°C$).

Table 2.   Transient heat transfer coefficients for Sn 5wt.% Pb cylindrical castings.

Position	Sn 5wt.% Pb	
	$T_P = 232°C$	$T_P = 270°C$
1 (Lateral)	$h = 2150t^{-0.27}$	$h = 3400t^{-0.38}$
2 (45°)	$h = 3950t^{-0.33}$	$h = 4950t^{-0.44}$
3 (Bottom)	$h = 4500t^{-0.25}$	$h = 8100t^{-0.37}$

Table 3.   Transient heat transfer coefficients for Sn 15wt.% Pb cylindrical castings.

Position	Sn 15wt.% Pb	
	$T_P = 217°C$	$T_P = 252°C$
1 (Lateral)	$h = 1200t^{-0.20}$	$h = 1800t^{-0.35}$
2 (45°)	$h = 2550t^{-0.32}$	$h = 2650t^{-0.32}$
3 (Bottom)	$h = 5300t^{-0.38}$	$H = 4500t^{-0.26}$

The variations of the heat transfer coefficient as a function of time are shown in figures 11–14. It can be seen that a significant difference on metal/mold heat transfer efficiency exists along the cross section of horizontal cylindrical castings. The *h* curves show that for all positions (1, 2, and 3) the heat transfer coefficient profiles drop rapidly as a result of gap formation at the initial stage of solidification, but then *h* reaches approximately a steady value. It can be seen that a significant difference in metal/mold heat transfer efficiency exists along the cross section of horizontal cylindrical castings. The difference is greater between positions 1 and 3, due to the progressive decrease
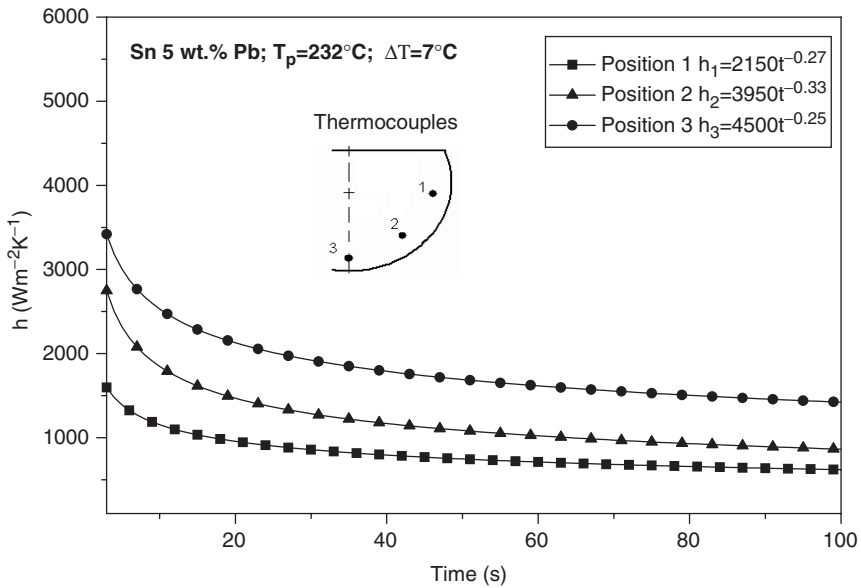
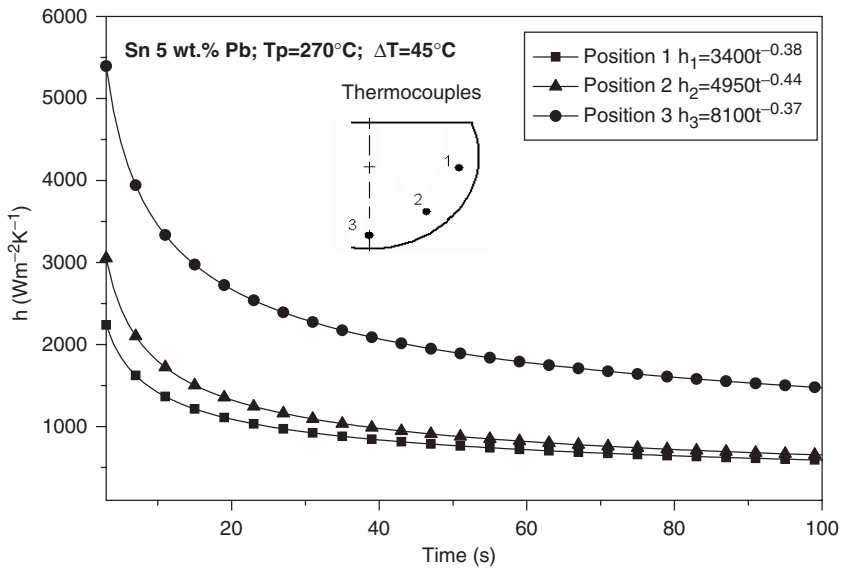Figure 11. Variation of the heat transfer coefficient with time (Sn 5wt.% Pb, $T_P = 232°C$).

Figure 12. Variation of the heat transfer coefficient with time (Sn 5wt.% Pb, $T_P = 270°C$).

of the gravitational influence. It can be seen that higher h profiles are obtained as the melt superheat is increased. Campbell reports that the fluidity of molten Sn–Pb alloys increases with increasing superheat, favoring the wetting of the chill by the melt [19]. This fact is more evident in the Sn 5 wt.% Pb than in the Sn 15 wt.% Pb alloy.

The influence of alloy composition on heat transfer coefficient is shown in figure 15 for the bottom position (position 3). Experiments performed in a vertical upward
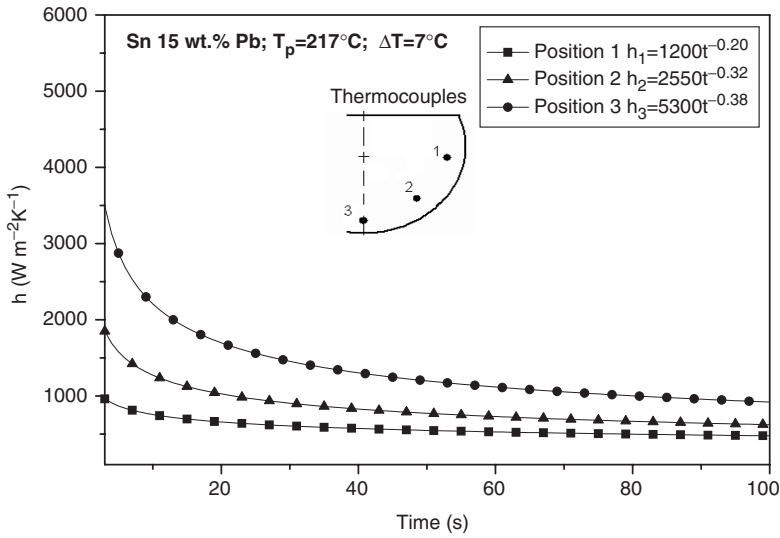
Figure 13.   Variation of the heat transfer coefficient with time (Sn 15wt.% Pb, $T_P = 217°C$).
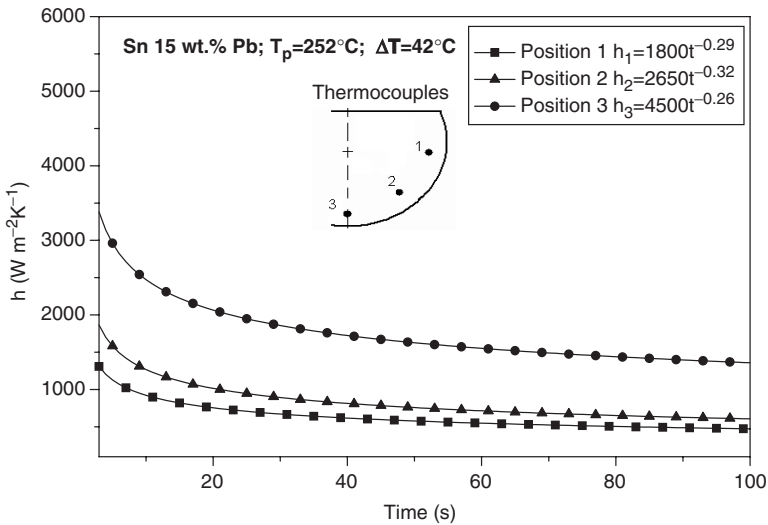

Figure 14.   Variation of the heat transfer coefficient with time (Sn 15wt.% Pb, $T_P = 252°C$).

solidification mold, also using Sn–Pb alloys [20], have shown a similar behavior of *h* profiles according to the alloy composition, i.e., lower *h* profiles are obtained as the solute concentration is increased.

5. Conclusions

Experiments were conducted to analyze the behavior of metal/mold heat transfer coefficients (*h*) during solidification of Sn–Pb alloys in a cylindrical stainless steel chill.
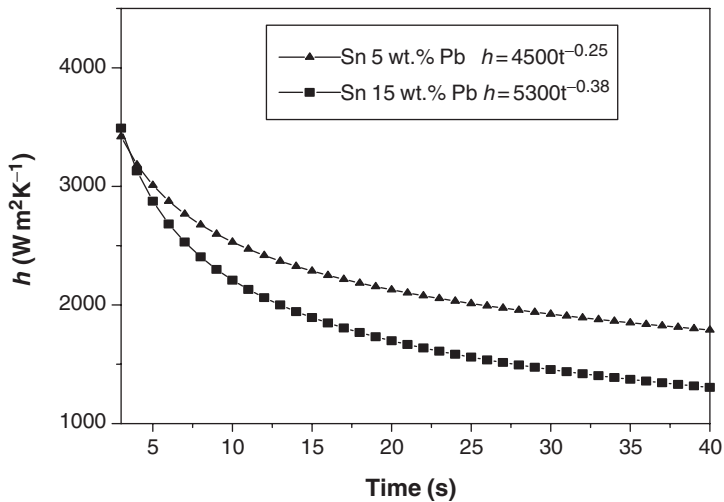
Figure 15. Heat transfer coefficient as a function of time for different alloy compositions: bottom part of the mold (position 3). Melt superheat: 3% above liquidus temperature.

The following conclusions can be drawn:

(1) The transient heat transfer coefficient has been characterized by using an approach based on the measured temperatures along casting and chill, and numerical simulations provided by a heat flow model based on IHCP procedure.

(2) The metal/mold heat transfer coefficients have been expressed as a power function of time, given by the general form:

$$h = at^{-b}$$

(3) The determination of heat transfer coefficients with angular position in cylindrical systems provides more precise solidification information useful for conventional foundry and continuous casting processes.

(4) The heat flow variation at the metal/mold interface is dependent on the thermal contraction, the gravitational effect and the alloy composition, and influences the morphology of the structure. The thermal contact is more effective at the bottom, decreasing along the cylinder surface toward the top of the mold.

Nomenclature

c = specific heat [J kg K^{-1}]
h = overall heat transfer coefficient [W m^{-2} K^{-1}]
h_i = interface heat transfer coefficient [W m^{-2} K^{-1}]
k = thermal conductivity [W m^{-1} K^{-1}]
K_o = partition coefficient
L = latent heat of fusion [J kg^{-1}]
$\dot{q}$ = internal heat generation [J kg^{-1}]
T = temperature [°C]
ΔT = melt superheat [°C]

T_E = eutetic temperature [°C]
T_F = fusion temperature [°C]
T_L = liquidus temperature [°C]
T_P = initial melt temperature [°C]
T_S = solidus temperature [°C
T_a = ambient temperature [°C]
t = time [s]
e = mold thickness [m]

Greek symbols

ρ = density [kg m^{-3}]

Subscripts

L = liquid
S = solid
W = water
m = mold
M/m = metal/mold

References

[1] Goudie, N.J. and Argyropoulos, S.A., 1995, Technique for the estimation of thermal resistance at solid metal interfaces formed during solidification and melting. *Canadian Metallurgical Quartely*, **34**, 73–84.
[2] Krishnan, M. and Sharma, D.G.R., 1996, Determination of the interfacial heat transfer coefficient *h* in unidirectional heat flow by Beck's non linear estimation procedure. *International Communications in Heat Mass Transfer*, **23**, 203–214.
[3] Lee, J.H., Kim, H.S., Won, C.W. and Cantor, B., 2002, Effect of the gap distance on the cooling behavior and the microstructure of indirect squeeze cast and gravity die cast 5083 wrought Al alloy. *Materials Science and Engineering A*, **338**, 182–190.
[4] Loulou, T., Artyukhin, E.A. and Bardon, J.P., 1999, Estimation of thermal contact resistance during the first stages of metal solidification process: I – experiment principle and modelisation. *International Journal of Heat and Mass Transfer*, **42**, 2119–2127.
[5] Martorano, M.A. and Capocchi, J.D.T., 2000, Heat transfer coefficient at the metal-mould interface in the unidirectional solidification of Cu–8%Sn alloys. *International Journal of Heat and Mass Transfer*, **43**, 2541–2552.
[6] Siqueira, C.A., Cheung, N. and Garcia, A., 2002, Solidification thermal parameters affecting the columnar-to-equiaxed transition. *Metallurgical and Materials Transactions A*, **33A**, 2107–2117.
[7] Santos, C.A., Siqueira, C.A., Garcia, A., *et al*., 2004, Metal-mold heat transfer coefficients during horizontal and vertical unsteady-state solidification of Al–Cu and Sn–Pb alloys. *Inverse Problems in Engineering*, **12**, 279–296.
[8] Fortin, G., Louchez, P.R. and Samuel, F.H., 1994, Evolution of the heat transfer during the radial solidification of pure aluminium. *La Revue of Métallurgie-CIT/Science et Génie gives Matériaux*, **91**, 771–780.
[9] Trovant, M. and Argylopoulos, S., 2000, Finding boundary conditions: a coupling strategy goes the modeling of metal casting process: part I. Experimental study and correlation development. *Metallurgical and Materials Transactions B*, **31**, 75–86.
[10] Kim, T.G. and Lee, Z.H., 1997, Time-varying heat transfer coefficients between tube-shaped casting and metal mold. *International Journal of Heat and Mass Transfer*, **40**(15), 3513–3525.
[11] Incropera, F.P. and Dewitt, D.P., 1990, *Fundamentals of Heat and Mass Transfer*, 3rd Edn (Singapore: John Wiley & Sons), p. 58.
[12] Santos, C.A., Quaresma, J.M.V. and Garcia, A., 2001, Determination of transient interfacial heat transfer coefficients in chill mold castings. *Journal of Alloys and Compounds*, **319**, 174–186.

[13] Siqueira, C.A., Cheung, N. and Garcia, A., 2003, The columnar to equiaxed transition during solidification of Sn–Pb alloys. *Journal of Alloys and Compounds*, **351**, 126–134.

[14] Beck, J.A., 1970, Nonlinear estimation applied to the nonlinear inverse heat conduction problem. *International Journal of Heat and Mass Transfer*, **13**, 703–716.

[15] Pehlke, R.D., Jeyarajan, A. and Wada, H., 1982, 1981, *Summary of Thermophysical Properties for Casting Alloys and Mold Materials* (Ann Arbor: University of Michigan).

[16] Toloukian, Y.S., *et al.*, 1970, *Thermal Properties of Matter*, Vol. 1 (New York: IFI/Plenum).

[17] Benjan, A., 1993, *Heat Transfer* (New York: Wiley).

[18] Bouchard, D. and Kirkaldy, J.S., 1997, Prediction of dendrite arm spacings in unsteady and steady-state heat flow of unidirectionally solidified binary alloys. *Metallurgical Transactions*, **28B**, 651–663.

[19] Campbell, J., 1991, *Castings* (London: Butherworth Heinemann).

[20] Rocha, O.F.L., Siqueira, C.A. and Garcia, A., 2003, Heat flow parameters affecting dendrite spacings during unsteady-state solidification of Sn–Pb and Al–Cu alloys. *Metallurgical and Materials Transactions*, **34A**, 995–1006.